Gradient drift instability and decameter ionospheric irregularities at the edge of polar holes

Scott Thaller*[1], Joe Hughes[1], Geoff Crowely[1], John Noto[1], Ryan Blay[1], Junk Wilson[1]

[1]Orion Space Solutions, Louisville, CO
Correspondence: scott.thaller@orionspace.com

Introduction

The polar and high latitude regions of the ionosphere are host to complex plasma processes involving Magnetosphere-Ionosphere (MI) coupling, plasma convection, and auroral dynamics. The magnetic field lines from the polar cusp down through the auroral region map out to the magnetosphere and project the footprint of the large-scale convective processes driven by the solar wind onto the ionosphere. This region is also a unique environment where the magnetic field is oriented nearly vertical, resulting in horizontal drifts along closed, localized, convection patterns, and where prolonged periods of darkness during the winter result in the absence of significant photoionization. This set of conditions results in unique ionospheric structures which can set the stage for the generation of the gradient drift instability (GDI). The GDI occurs when the density gradient and ExB plasma drift are in the same direction, as illustrated in Figure 1.

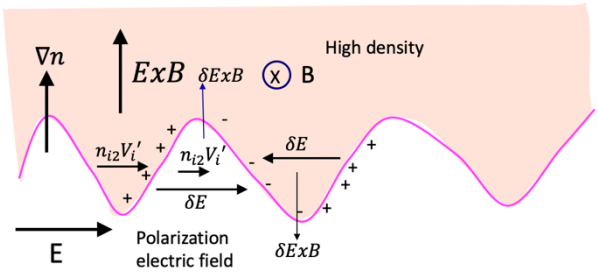

***Figure 1**: The gradient drift instability (GDI) occurs where the plasma density gradient is aligned with the ExB convective plasma drift. Under these conditions, small perturbations on the boundary are amplified due to the perturbation electric field, δE.*

The GDI is a source of structuring at density gradients and may give rise to ionospheric irregularities that impact over-the-horizon radars and GPS signals. While the plasma ExB drifts are supplied by magnetospheric convection and MI coupling, sharp density gradients in the polar regions will be present at polar holes. Polar holes are large, ~1000 km, ionospheric structures with a maximum plasma density at least a factor of three lower that the daily average maximum. Polar holes tend to form during polar winter during periods of low geomagnetic activity when ionospheric convection proceeds slowly. Since the GDI occurs where the density gradient and plasma drift are parallel, the ionospheric irregularities caused by the GDI should occur at the leading edge of the polar hole. If so, the resulting production of small-scale density irregularities may, if the density is high enough, give rise to scintillation of GNSS signals and backscatter on HF radars. These effects have been observed on the steep gradients at the edge of polar patches, which are large localized enhancements of ionospheric plasma density. Thus, in addition to being a rich area for scientific research, polar holes and convective

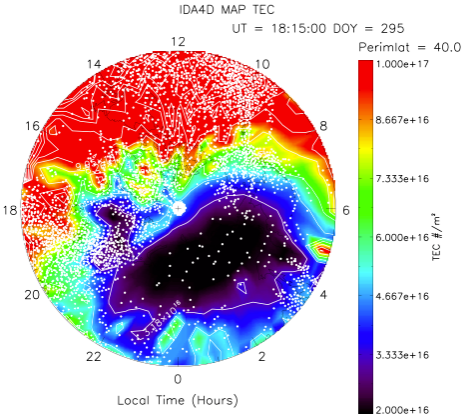

***Figure 2**: Example of IDA4D TEC from 10/22/2019/ The white dots show the pierce points of the TEC rays.*

processes may have important implications for GPS/GNSS positioning, navigation, and timing (PNT), and for radar detection and ranging.

In this study, we investigate whether these irregularities can occur at the edges of polar holes as detected by the HF radar scatter. We use the Ionospheric Data Assimilation 4-Dimentional (IDA4D) and Assimilative Mapping of Ionospheric Electrodynamics (AMIE) models to characterize the high latitude ionospheric density and ExB drift convective structures, respectively, for one of nine polar hole events identified using RISR-N incoherent scatter radar in Forsythe et al [2021]. The combined IDA4D and AMIE assimilative outputs indicate where the GDI could be triggered, e.g., locations where the density gradient and ExB drift velocity have parallel components and the growth rate is smaller than the characteristic time over which the convective pattern changes, in this case, ~1/15 min. The presence of decameter ionospheric plasma irregularities is detected using the Super Dual Auroral Radar Network (SuperDARN). SuperDARN radars are HF coherent scatter radars. The presence of ionospheric radar returns in regions unstable to GDI grown strongly suggest the GDI is producing decameter scale plasma irregularities.

Datasets

The polar hole event investigated in this study were previously identified by Forsythe et al [2021] using the Resolute Bay (RISR) and Poker Flat (PFISR) Incoherent Scatter Radars. In this study, we focus on the polar hole event of 22 October 2019. To identify where the ionosphere is unstable to the GDI we need the ionospheric density and ExB convective drift. To determine the presence of decameter-scale ionospheric irregularities, we need to observe HF ionospheric radar backscatter. Specifically, the GDI should produce magnetic field aligned structuring of the ionosphere. This adds a constraint to the scatter observations that the ray be near (+/- 5o) to the magnetic field. The datasets and associated tools are:

1. *Ionospheric electron density* from the Ionospheric Data Assimilation Four-Dimensional (IDA4D) model. IDA4D is an assimilative model of the ionosphere. In this study, IDA4D was run ingesting *Total Electron Content* (TEC) from a variety of GNSS signals, giving excellent coverage of the high latitude regions. See Figure 2 for an example of IDA4D TEC.
2. *Plasma ExB drift* from the Assimilative Mapping of Ionospheric Electrodynamics (AMIE) is an assimilative model of the middle and high latitude (>40^o magnetic latitude) ionospheric electric field. In this effort AMIE ingests *DMSP ion drifts*, SuperDARN *ExB convection patterns*, and *ionospheric current* proxies from ground magnetometer data and uses the Weimer model as the background for assimilation. Figure 3 shows the AMIE plasma ExB drift convection pattern as equipotential contours at latitudes above 40^o magnetic.
3. *The location of decameter-scale ionospheric density irregularities* detected by Super Dual Auroral Radar Network (SuperDARN). Ionospheric scatter only is used. Figure 4 shows an example of SuperDARN data with ionospheric and ground scatter distinguished. In

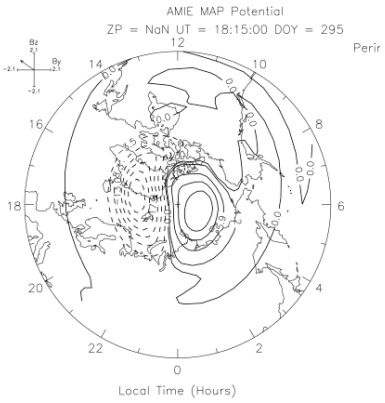

***Figure 3**: Example of the AMIE equipotential contours, which follow the ExB drift paths. The typical two-cell convection pattern is apparent.*

addition, as noted above SuperDARN data are used in AMIE as source of convective measurements.

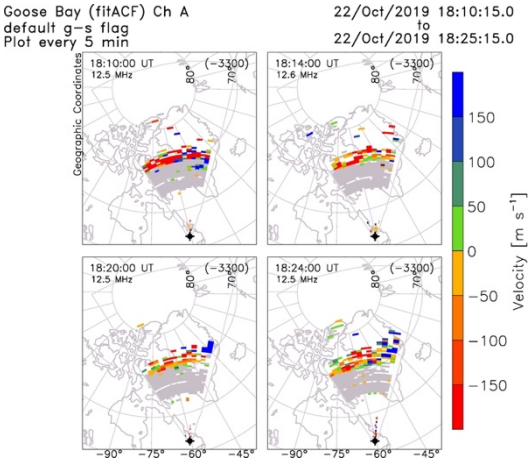

***Figure 4**: Example SuperDARN Goose Bay radar velocity, indicating returns from the ionosphere (colored) and ground (grey) for 18:10-18:24 UT 10/22/19. Generated by vt.superdarn.org*

For this investigation, we are using IDA4D ionospheric density and AMIE ExB on a 3º latitude x 3º longitude grid and 15-minute time steps. This gridding best suited the IDA4D output. We bin the SuperDARN radar return power by the same grid and temporal resolution we used for AMIE and IDA4D. To each grid cell we assign the median radar scatter power that falls within that cell over the 15-minute duration. We take the GDI inverse growth rate from the altitude range of 100 to 400 km and collapse these into a single latitude-longitude map for each 15-minute time step. For those maps, we choose the fastest growth rate per lat-lon cell over that altitude range. Figure 5 shows an example of how these several datasets are combined.

GDI and Radar Scatter Statistics for 22 October 2019

Using the whole day of 22 October 2019, we have conducted two different statistical analyses on the radar scatter and GDI growth rates. One, shown in Figure 6, separates the "high" from "low" return powers, as defined as greater and less than the median power. Then we select all the GDI growth rates that coincide with "high" radar power return as one population and the GDI growth rates that coincide with "low" power as a second, separate population. If the higher return power is due to more scatter caused by the GDI, then the population of the GDI growth rates taken from location with high radar return power should be more skewed towards larger values (or shorter growth times). The second analysis method, shown in Figure 7, takes the GDI coincident with any scatter (regardless of power) and compares the distribution of growth times in that population to those coincident with regions of no detected scatter. If a faster GDI growth creates structuring that increases the backscatter power, then the occurrence histogram of the GDI growth times should shift towards faster rates when using GDI values that coincide with scatter, verse the general GDI population regardless of whether scatter is present or not.

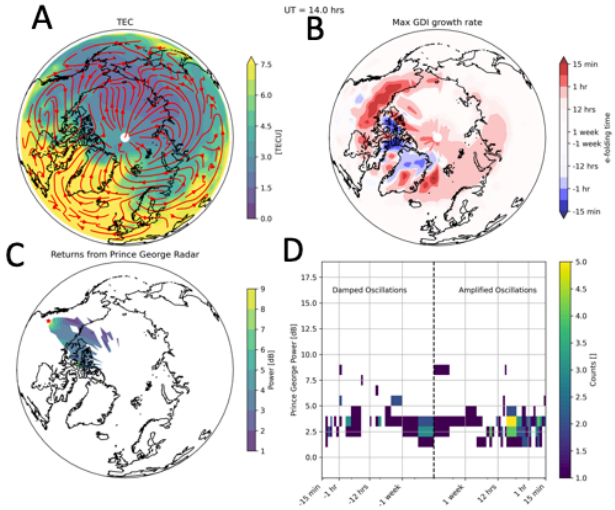

***Figure 5**: Combined view of the datasets for 14:00 – 14:15 UT on 10/22/19. 4A shows a TEC map with ExB drift contours overlaid. 4B shows the GDI e-folding growth time (inverse growth rate). Red indicates where the ionosphere is unstable to the GDI, blue where it is stable. 4C show the Price George SuperDARN radar scatter, and 4D shows 2D histogram of radar scatter power and GDI growth time.*

Figure 6 shows the results of the first statistical comparison described above. The distributions of GDI growth times (inverse growth rate) collocated

with high (low) scatter power in orange (blue). The two distributions are similar, indicating that the two chosen power levels of SuperDARN HF scatter does not sort the GDI growth rate. Experiments with different bin widths and GDI ranges show similar results. It is important to note that the scatter power from the GDI induced structuring is expected to be field aligned, meaning the scatter will be strongest when then radar ray is perpendicular to the magnetic field. The data used in Figure 6 was not filtered by ray angle relative to the magnetic field. It is possible that scatter from non-perpendicular rays obscures effects of the GDI. Figure 7 show the result of the second method described above. In Figure 7 we compare three distributions of the GDI growth times. The first of the three distributions is shown in blue; in this distribution the GDI growth times from the region observed by SuperDARN are selected but with no scatter-based selection criteria (all GDI growth rate values in the observation area). The second distribution (shown in green) are the GDI values selected only where ionospheric scatter (of any power) is observed. The third distribution is made from the GDI values where there is both scatter and the ionospheric density at 300km is high enough to refract the ray to being perpendicular to the magnetic field. This density as a function of elevation angle is estimated using Snell's law and the geometry of a ray launched at a given elevation, using a method similar to that described in Ponomarenko et al [2011], and piercing the ionosphere at 300 km on a curved Earth. Comparing the blue and green distributions reinforces the conclusion of Figure 6; selecting GDI growth rates by the presence of scatter does not alter the shape of the distribution. Comparing the overall growth rate distribution (red) to the other two, we see that this distribution has a shape that resembles the other two. This shows that selecting GDI growth rates concurrent with scatter in regions where the ray should be near perpendicular does not result in a distribution skewed towards faster (and positive) growth rates. Such a skewing may be expected if the faster growth rates resulted in a greater amplitude of the ionospheric density irregularities at decameter scales.

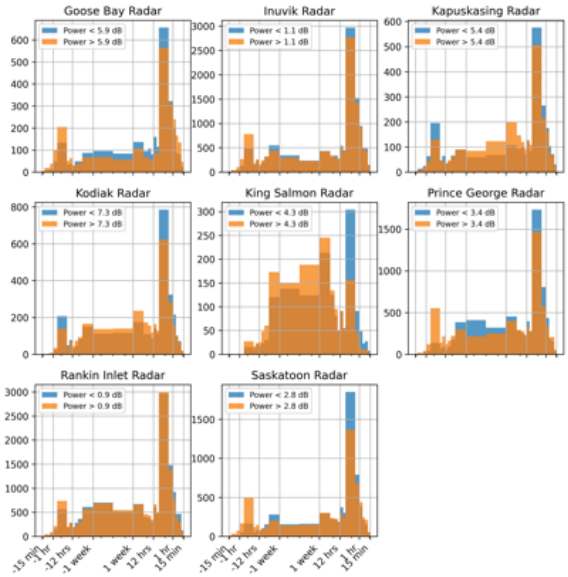

***Figure 6**: The distributions of the GDI e-folding growth time for high and low scatter power over 10/22/19, for eight radars.*

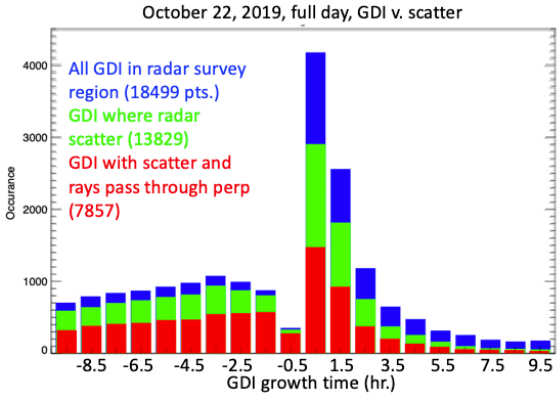

Figure 7: Three distributions of the GDI growth time (inverse growth rate) for 10/22/19 when then growth rate values are selected from (A) the region observed by SuperDARN (blue); (B) the GDI growth rates that coincide with scatter (green); and (C) the GDI growth rate that coincides with both scatter and ionospheric density high enough to refract the ray to perpendicular to the magnetic field (red).

Discussion and Conclusions

In both of the two statistical analyses described above, shown in Figures 6 and 7, we concluded that the distribution of GDI growth rates is not changed when selecting the growth rate values based on HF scatter. If a faster GDI growth rate results in

larger amplitude density structures at the appropriate scattering size (decameter), then enhanced scatter power should be observed there. This is especially true then the ray is perpendicular to the magnetic field, which is the optimal geometry for detecting field aligned irregularities. The return power, P, goes as the mean amplitude of the density irregularities, the latter being proportional the background density $P \propto <\delta N^2> \propto N^2$ [Ponomarenko et al., 2011]. Perhaps at the edges of polar holes, the plasma that is formed into the decameter scale irregularities is of too low a density to cause significant scattering. A study by Jenner et al [2020] found a lack of GNSS phase scintillations at the edge of polar holes. They concluded that this was likely due to the low density. It may be that a similar effect limits the ability of HF radars to detect that expected scatter.

The statistical analyses conducted in the above investigation do not show a clear pattern of enhanced scatter with faster GDI growth rates. Further investigation mush be conducted before concluding that the GDI does not cause irregularities detectable with HF radar at polar holes. First, we have seven other polar hole events to investigate. Second, there are other statistical methods we have yet to apply to the study. For example, using the quantities of peak power, standard deviation of power, etc. Third, more careful ray tracing analysis to ensure the ray is close to orthogonal to the background magnetic field can be deployed. Fourth, while the strongest density gradients do tend to be at the edge of the polar holes, the analyses dataset also included large gradients elsewhere. Further analysis that limits the regions explored to the actual edge of polar holes is forthcoming. In a preliminary analysis we looked at the locations where the ionosphere is unstable to GDI, ionospheric scatter is observed, and the ray should be refracted to perpendicular. About ~60% of these locations were located near the leading edge of the polar hole. In addition, OSS is developing a couple model for improved specifications of ionospheric density structure and electrodynamics. This new tool will more accurately identify the locations where ionospheric instabilities are prone to developing.

Acknowledgements
'The authors acknowledge the use of SuperDARN data. SuperDARN is a collection of radars funded by national scientific funding agencies of Australia, Canada, China, France, Italy, Japan, Norway, South Africa, United Kingdom and the United States of America.'

References

Forsythe, V. V., Kunduri, B., & Zou, S. (2021). Multi-instrument investigation of the polar holes. Journal of Geophysical Research: Space Physics, 126, e2021JA029795. https://doi. org/10.1029/2021JA029795

Jenner et al (2020) Plasma density gradients at the edge of polar ionospheric holes: the absence of phase scintillation Ann. Geophys., 38, 575–590, 2020 https://doi.org/10.5194/angeo-38-575-2020

Ponomarenko, P. V., A. V. Koustov, J.-P. St.-Maurice, and J. Wiid (2011), Monitoring the F-region peak electron density using HF backscatter interferometry, Geophys. Res. Lett., 38, L21102, doi:10.1029/2011GL049675.